Journal of Solid State Chemistry 183 (2010) 1917–1924

Contents lists available at ScienceDirect

Journal of Solid State Chemistry

journal homepage: www.elsevier.com/locate/jssc

Nonaqueous seeded growth of flower-like mixed-phase titania nanostructures for photocatalytic applications

Yu-Chuan Hsu, Huang-Ching Lin, Chia-Hsiu Chen, Yi-Ting Liao, Chia-Min Yang*

Department of Chemistry, National Tsing Hua University, Hsinchu 30013, Taiwan

ARTICLE INFO

Article history:
Received 10 April 2010
Received in revised form
19 June 2010
Accepted 24 June 2010
Available online 30 June 2010

Keywords:
Mixed-phase titania
Seeded growth
Nonaqueous synthesis
Flower-like nanostructure
Photocatalyst

ABSTRACT

A nonaqueous seeded-grown synthesis of three-dimensional TiO_2 nanostructures in the benzyl alcohol reaction system was reported. The synthesis was simple, high-yield, and requires no structural directing or capping agents. It could be largely accelerated by applying microwave heating. The TiO_2 nanostructures had a unique flower-like morphology and high surface area. Furthermore, the structural analyses suggested that the nanostructures had a non-uniform distribution of crystalline phases, with the inner part rich in anatase and the outer part rich in rutile. After heat treatments, the mixed-phase TiO_2 nanostructures exhibited high photocatalytic activities for the photodegradation of methylene blue as compared to Degussa P25. The high photoactivities may be associated with the high surface area and the synergistic effect resulting from the anisotropic mixed-phase nanostructures. The results demonstrate the uniqueness of the nonaqueous seeded growth and the potential of the TiO_2 nanostructures for practical applications.

1. Introduction

Titanium dioxide (titania, TiO_2) is a wide band-gap semiconductor material with high stability, high photoactivity and low cost. Owing to these properties, TiO_2 has been widely applied in the fields of dye-sensitized solar cells [1–4] and the photodegradation of organic pollutants in water and in air [5–16]. The photocatalytic activity of TiO_2 is mainly dependent on the crystalline phase and its crystallinity. Anatase usually demonstrates higher activity than rutile because of a greater extent of electron–hole recombination in rutile [17,18]. However, rutile has a smaller band gap than anatase and has a photo-response extending slightly into the visible light region. When mixing the two phases together, the resulting mixed-phase materials may exhibit a synergistic effect leading to better photocatalytic activity than pure-phase anatase [19–23]. In addition, photocatalytic reactions occur on the titania surface and therefore high surface area usually leads to high photoactivity. High-surface-area titania materials include mesoporous TiO_2 powders and films [8,10,15,24,25] and three-dimensional (3D) TiO_2 nanostructures composing of nanotubes, nanowires, nanosheets and nanoparticles [14,26–28].

The preparations of most of these TiO_2 materials involve aqueous sol–gel chemistry [29]. Generally, the reaction parameters in the aqueous sol–gel synthesis are difficult to control [30,31], and the high complexity of synthesis solutions leads to a situation in which slight changes in experimental conditions have a strong influence on particle morphology [32,33]. Moreover, the thus prepared materials are generally amorphous or poor in crystallinity. Subsequent heat treatment is often necessary to induce crystallization or to improve the crystallinity of the materials [8,10,15], but this additional step results in alteration, mainly particle growth, or even destruction of the well-defined particle morphology. Methods have been developed to prepare TiO_2 nanomaterials simultaneously possessing crystalline phase and high surface area, but complicated and time-consuming processes and/or the utilization of structure-directing or capping agents are often necessary [8–10,14,15,24–28].

Nonaqueous sol–gel routes are a valuable alternative and are able to overcome many of the aforementioned problems typical for the aqueous sol–gel systems [34–39]. Among them, the reaction system of benzyl alcohol and metal chlorides is a versatile process [38–42]. The reaction system can produce anatase TiO_2 and other metal oxide nanoparticles with high crystallinity at relatively low temperatures, and the crystal growth in the reaction system can also be controlled without the use of surfactants [38–42]. By applying the benzyl alcohol reaction system, we herein report a simple and high-yield synthesis of mixed-phase and high-surface area TiO_2 nanostructures with a flower-like morphology by a seeded growth without using any structure-directing agents or capping agents. We also found that materials with similar structural and morphological properties could be synthesized within hours by applying a microwave heating. The effects of synthesis conditions and

* Corresponding author. Fax: +886 3 5165521.
E-mail address: cmyang@mx.nthu.edu.tw (C.-M. Yang).

0022-4596/$ - see front matter © 2010 Elsevier Inc. All rights reserved.
doi:10.1016/j.jssc.2010.06.016

subsequent heat treatment on the structure and morphology of the materials were studied. In addition, the photocatalytic activity of the TiO_2 materials was evaluated by the photodegradation of methylene blue, a model pollutant in semiconductor photocatalysis [43–46]. Compared to the commercial mixed-phase TiO_2 Degussa P25, most of the flower-like TiO_2 nanostructures were found to exhibit higher photocatalytic activity. Moreover, owing to their 3D flower-like morphology, the TiO_2 nanostructures could be easily filtered and separated from the solution without the need of centrifugation. The results demonstrate the uniqueness of the nonaqueous seeded growth for the preparation of 3D TiO_2 nanostructures for practical applications.

2. Experimental section

2.1. Seeded growth of TiO_2 nanostructures

The commercial mixed-phase P25 (Degussa, Germany) or pure-anatase ST21 (Ishihara Sangyo, Japan) TiO_2 nanoparticles were used as seeds for the growth of TiO_2 nanostructures. The seed nanoparticles were dispersed in benzyl alcohol (BA) in a nitrogen atmosphere, and $TiCl_4$ was then added dropwise under vigorous stirring at room temperature. The synthesis mixture was stirred in an oil bath at 80 °C for 24 h. The molar composition of the synthesis mixture was 1.0 $TiCl_4$: x seeds: 20.0 BA, where x (x=0.1–2.0) is the equivalent molar ratio of TiO_2 seeds. The products were washed with chloroform and ethanol and were then dried at 60 °C. Selected samples were further heated at 300–500 °C in air for 1 h using a temperature ramp of 1 °C min^{-1}. The as-synthesized samples are designated as SGP-x (seeded with P25) or SGS-x (seeded with ST21), and the samples thermally treated at temperature T are designated as SGP-x-T or SGS-x-T. The seeded growth with microwave heating was also performed. A synthesis mixture with x=0.3 was prepared and was transferred to a Teflon reaction vessel. The mixture was then subjected to microwave heating at 100 °C for 1 h using a CEM MARS microwave digestion system operating at a frequency of 2.45 GHz. The resulting sample was designated as mSGP-0.3.

2.2. Characterization

Powder X-ray diffraction (PXRD) patterns were recorded on a Mac Science 18MPX diffractometer using Cu $K\alpha$ radiation. The crystallite sizes of the anatase and rutile phases were calculated from the line broadening of the (101) reflection of anatase and (110) reflection of rutile by using the Scherrer equation. The weight fractions of the two phases were estimated from the integrated intensities of the anatase (101) and rutile (110) reflections by applying the formula reported by Zhang and Banfield [47]. For the seeded-grown samples, the reflections have contributions from both the seeds and the newly grown TiO_2, and therefore they were deconvoluted into two sets of reflections, one with the peak widths and intensities identical to those for the seeds, for the analyses of crystallite sizes and phase contents. Scanning electron microscopy (SEM) images were recorded on a JEOL JSM-7000F microscope operating at 10 kV, and transmission electron microscopy (TEM) images were taken using a JEOL JEM-2010 microscope operated at 200 kV. Nitrogen physisorption isotherms were measured at 77 K using a Quantachrome Autosorb-1MP volumetric adsorption analyzer. Thermogravimetric analysis was performed using a Linseis STA PT1600 analyzer. UV–visible absorption spectra were recorded on a JASCO V-650 spectrophotometer equipped with a diffuse reflection accessory.

2.3. Photocatalytic decomposition of methylene blue

An aqueous methylene blue (MB) solution with a concentration of 1.2×10^{-5} M was prepared. The solution pH was adjusted to ~6.5. The MB solution (200 mL) was poured in a quartz reactor, and the TiO_2 photocatalyst (25 mg) was then added and dispersed in the solution. After stirring in the dark for 6 h to reach the adsorption equilibrium, and solution was irradiated using an Oriel 150 W xenon lamp equipped with a UV bandpass filter (FSR-UG11, Newport, bandwidth of 200–400 nm). The power density of the UV irradiation on the solution was measured 1.7 mW cm^{-2}. The decomposition proceeded under aerobic (oxygen-saturated) conditions. After irradiation, the catalyst was removed by simple filtration (for 3D TiO_2 nanostructures) or by centrifugation (for P25 or ST21), and the amount of MB was determined by measuring the optical absorbance of the dye at 665 nm.

3. Results and discussion

All the seeded growth preparations had yields of 95–99% based on the weight of TiO_2 in the products. A heating time of 24 h was found to be the minimum to complete reactions in an oil bath. The seeded growth with a heating time of 2 h gave yields less than 10%, and the reactions heating for 6 h generally produced ~40% of the products. The PXRD patterns of P25 and the P25-seeded TiO_2 nanostructures (SGP-x samples) are shown in Fig. 1a. P25 TiO_2 is a mixed-phase material [48], and the PXRD analysis suggests a composition of 80% anatase and 20% rutile for the P25 seeds used in this study. All the SGP-x samples also contain both anatase and rutile phases. As the amount of the seeds decreased (with decreasing x), the relative intensities of the anatase reflections decrease while the reflections of rutile become more intense but broader. The PXRD patterns of the seeded-grown samples have contributions from both the P25 seeds and the newly grown TiO_2. In order to separate the contribution from the P25, the PXRD patterns were deconvoluted into two sets of peaks with different widths and intensities. One set of the deconvoluted pattern was attributed to P25 and the other was from the newly grown TiO_2, from which the crystallite size and phase content could be estimated by assuming a TiO_2 yield of 98%. The results, as shown in Table 1, suggest that the newly grown TiO_2 in all the SGP-x samples contain both anatase and rutile phases with very small (4–6 nm) crystallite sizes. The content of nanocrystalline rutile phase increases with decreasing the seed amount except for SGP-0.1. Similar phenomena were also observed when the pure-anatase ST21 nanoparticles were applied as seeds, and the corresponding PXRD patterns and the same structural analyses of the resulting mixed-phase SGS-x samples are shown in Fig. 1b and Table 1, respectively.

The mixed-phase SGP-x samples were characterized by SEM, and the images are shown in Fig. 2. The image of SGP-2.0 is quite similar to that of P25, which is composed of spherical nanoparticles with diameters of 20–30 nm. SGP-0.7 also mainly contains spherical nanoparticles, and in addition some needle-shaped nanoparticles are observed. Interestingly, further decrease of the seed amount resulted in the formation of 3D flower-like nanostructures in SGP-0.3, as shown in Fig. 2d. The magnified image (Fig. 2e) further shows that the nanostructures are around 200 nm in size and are composed of bundles of needle-shaped nanorods. When the seed amount was again decreased, the shape of the nanostructures became cauliflower-like, as demonstrated by the image of SGP-0.1 (Fig. 2f). The SGP-x samples were also subjected to nitrogen physisorption measurements, and the adsorption branches in the relative pressure range of 0.05–0.20

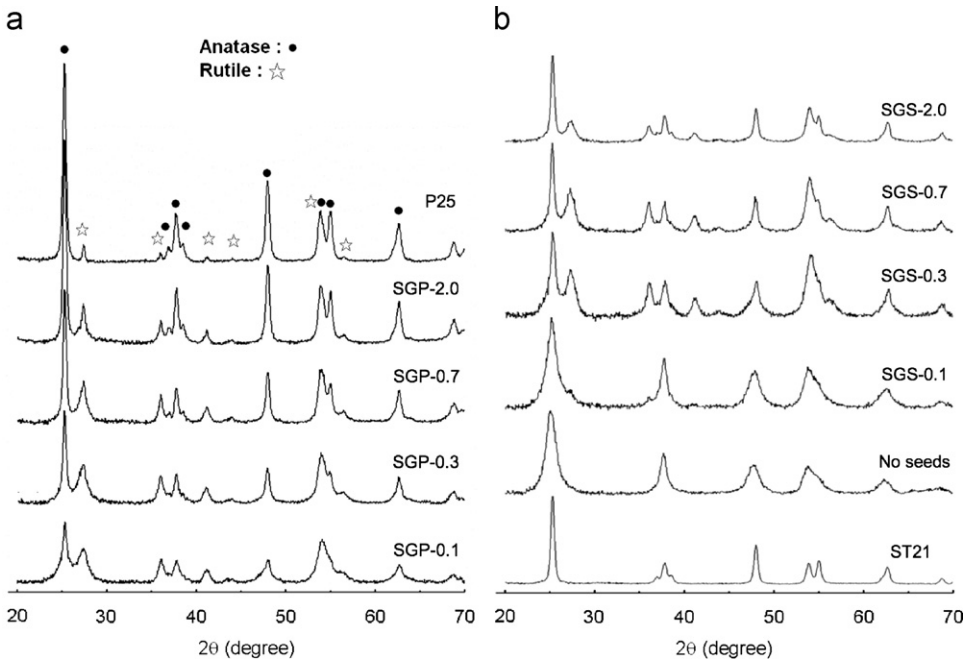

Fig. 1. (a) PXRD patterns of P25 and SGP-*x* samples. Reflections of anatase and rutile are indicated, respectively. (b) PXRD patterns of ST21, SGS-*x* samples and the sample synthesized without adding seeds.

Table 1
Estimated crystallite size and phase content of newly grown TiO_2 in selected samples.[a]

Samples	Anatase		Rutile		Samples	Anatase		Rutile	
	D (nm)	*W* (%)	*D* (nm)	*W* (%)		*D* (nm)	*W* (%)	*D* (nm)	*W* (%)
P25	23[b]	80[b]	20[b]	20[b]	ST-21	20[b]	100[b]		
SGP-2.0	ND[c]	55	4	45	SGS-2.0	ND[c]	48	5	52
SGP-0.7	4	45	5	55	SGS-0.7	5	38	5	62
SGP-0.3	6	36	5	64	SGS-0.3	5	42	5	58
SGP-0.1	6	42	5	58	SGS-0.1	6	96	ND[c]	4

[a] D: crystallite size; W: phase content.
[b] Values for the seed nanoparticles.
[c] Not determined.

were used to calculate their surface areas by applying the Brunaru–Emmett–Teller (BET) method. The obtained values for the SGP-*x* samples are in the range of 60–142 $m^2\ g^{-1}$, and SGP-0.3 has the highest surface area of 142 $m^2\ g^{-1}$. For comparison, P25 has a surface area of 50 $m^2\ g^{-1}$.

The amount of P25 seeds for SGP-0.3 was found optimum for the formation of the 3D flower-like morphology, and the sample was further characterized by TEM. As shown in Fig. 3a and b, the flower-like nanostructures in SGP-0.3 are quite uniform and are about 150–250 nm in size. Densely packed nanorods, about 60–120 nm in length and 4–5 nm in width, are clearly observed in each aggregate. The darker contrast at the center of each aggregate, most likely attributing to the P25 seed, is also observed. The shape of the nanorods does not have straight sides (cf. Fig. 3c), suggesting that the nanorods are not single crystalline but rather are composed of interconnected nanocrystals. Although the attempts to observe the lattice fringes failed due to the dense packing of nanorods, selected area electron diffraction (SAED) measurements provide interesting structural information of the sample. Fig. 3d shows the SAED pattern of the tips of the nanorods (corresponding to the image shown in Fig. 3c). All the diffraction spots are broad, indicating the nanocrystalline nature of the sample, and they can be indexed solely by the rutile phase. Therefore, the structural analyses of PXRD and SAED suggest that the flower-like mixed-phase TiO_2 nanostructures in SGP-0.3 may have a non-uniform distribution of the two crystalline phases, with inner part rich in anatase and outer part rich in rutile phase. It has to be mentioned that most of the reported synthetic strategies to prepare flower- or urchin-like TiO_2 nanomaterials need to apply structure-directing agents, surfactants, capping agents or hydrogen fluoride [14,26–28,54–56]. Flower-like rutile or mixed-phase agglomerates have also been obtained by thermal transformation of pure brookite nanostructures synthesized by modified thermolysis of titanium powders [57]. Compared to them, the nonaqueous seeded growth is relatively simple, efficient and needs no structure-directing or capping agents. In addition, the anisotropic mixed-phase structure in the resulting TiO_2 nanostructures is unique.

The formation of the extended and anisotropic 3D nanostructures of mixed-phase TiO_2 in the present study was in a nonaqueous BA reaction system [38–42]. A true "seeded" growth was confirmed by the SEM and TEM investigations, but the formation of rutile in addition to anatase phase was contradictory to the previous reports on the production of pure-anatase nanocrystals in the BA/$TiCl_4$ systems [38–42,49]. The control synthesis without any seeds was also performed, and indeed it solely produced anatase nanocrystals (cf. Fig. 1b). The fact that all

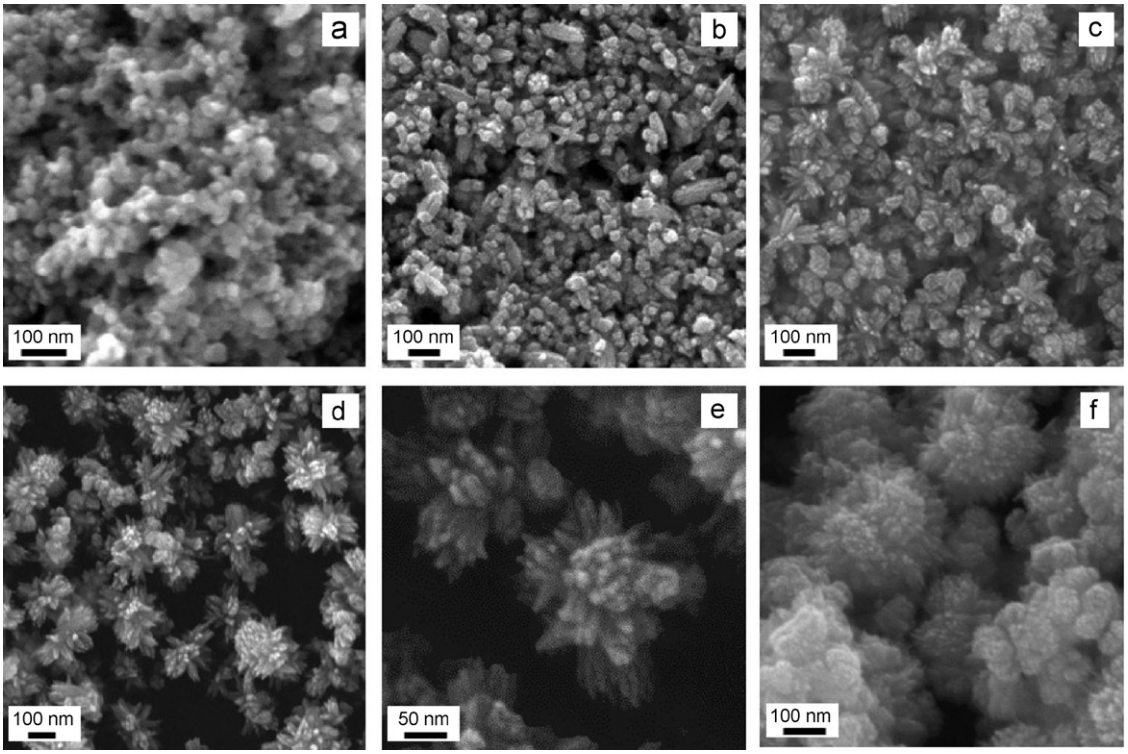

Fig. 2. SEM images of (a) P25, (b) SGP-2.0, (c) SGP-0.7, (d, e) SGP-0.3 and (f) SGP-0.1.

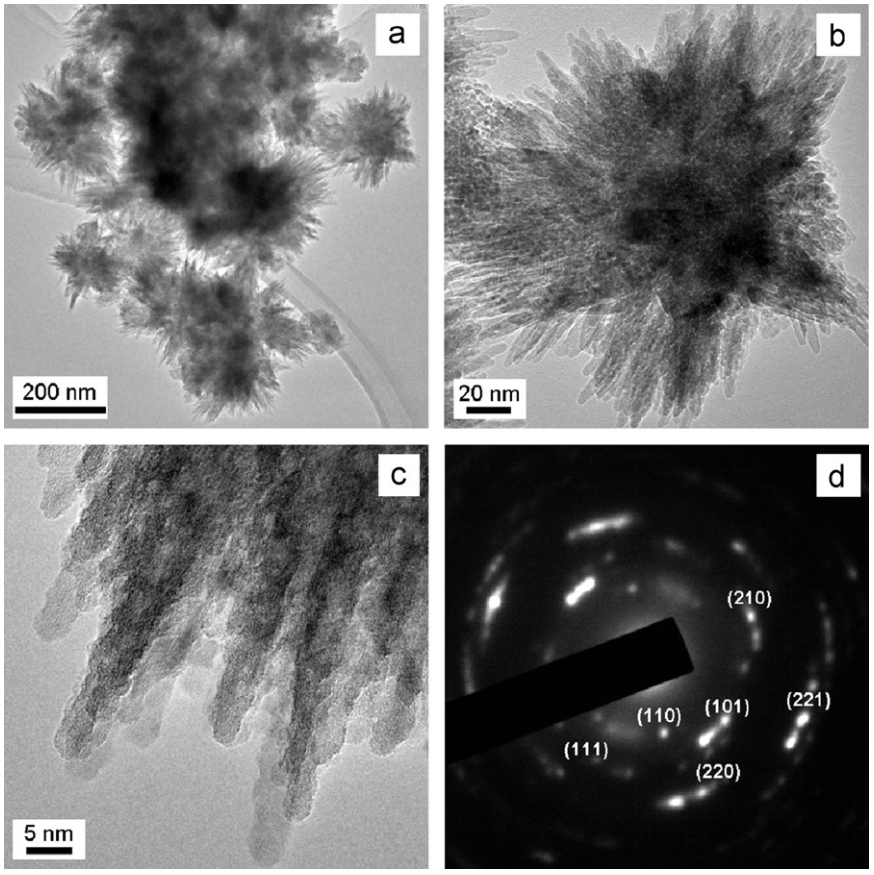

Fig. 3. (a–c) TEM images and (d) SAED pattern of SGP-0.3.

the seeded grown samples contain newly grown rutile, regardless of the type of seeds, implies that the structure-directed growth on the exposed surface of the same phase to have minimized lattice mismatch [7,14,26] may not be likely to happen. On the other hand, it has been reported that acidic medium of hydrochloric acid (HCl) or other acids would favor the formation of rutile phase [50–53]. Based on the fact that both the P25 and ST21 seeds are highly hydrophilic and have high density of surface titanol (Ti–OH) groups, we therefore speculate that $TiCl_4$ would react with the titanol groups and the water molecules adsorbed on the seed surface after being added into the BA solution. The reaction produced mainly nanocrystalline anatase on the seeds and HCl as a by-product. As the nonhydrolytic condensation proceeded, a concentration gradient of HCl around the seed was then developed, creating an environment probably more favorable for the growth of rutile nanocrystals. The proposed mechanism may account for the formation of the unique 3D mixed-phase TiO_2 nanostructures, and further study and examination is necessary.

The nonaqueous seeded growth could be even more efficient when a microwave heating is applied. This was demonstrated by a synthesis using P25 as the seeds ($x=0.3$) at 100 °C. The microwave-assisted growth only took an hour to give a yield of ~98%, and the structural and textural properties of the resulting sample (designated as mSGP-0.3) were very similar to those of SGP-0.3. As shown in Fig. 4, the PXRD pattern is indicative of the coexistence of anatase and rutile phases, and the relative intensities and widths of the reflections are comparable to those of the oil bath-heated sample SGP-0.3. For the newly grown TiO_2 in mSGP-0.3, the crystallite sizes were estimated to be ~5 nm for both anatase and rutile phases and the content of anatase was about 38%. Moreover, the TEM image reveals that mSGP-0.3 also contains flower-like aggregates, slightly smaller in size as compared to those in SGP-0.3. Therefore, the microwave-assisted seeded growth may be applied for large-scale preparation of the unique 3D mixed-phase TiO_2 nanomaterials.

It has been shown that the TiO_2 nanoparticles synthesized in the BA reaction system may have organic groups (derived from BA, such as benzyl groups) and BA adsorbed on the surface [58,59]. Indeed, thermogravimetric analysis suggested that the as-synthesized 3D TiO_2 nanostructures contained ~5–10 wt% organic residues, which could be completely decomposed and removed by a heat treatment at or above 300 °C. On the other hand, heat treatment may also affect the structure, morphology

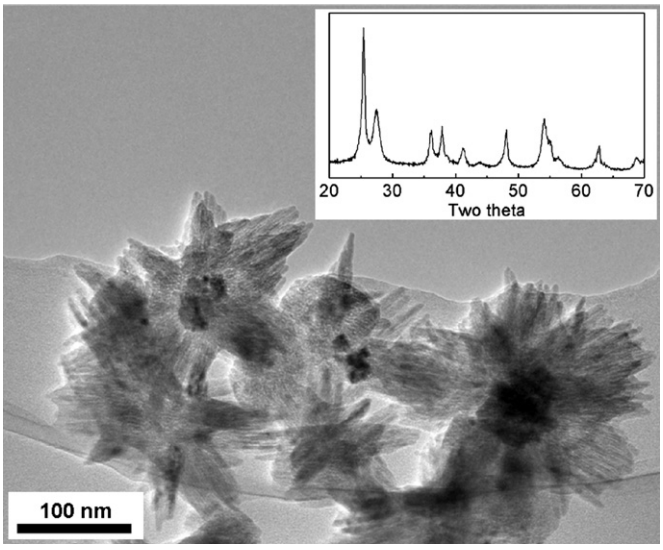

Fig. 4. PXRD pattern and TEM image of mSGP-0.3.

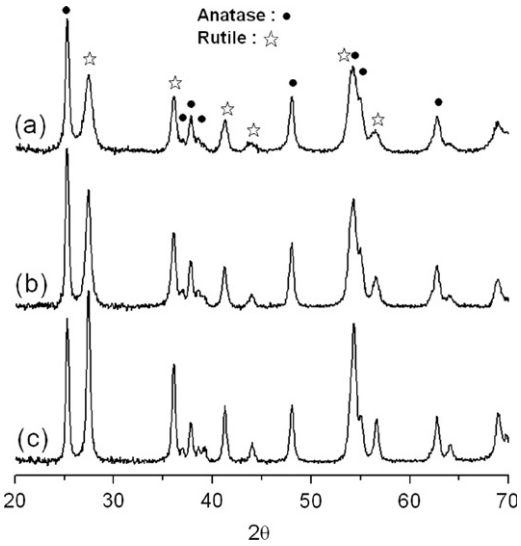

Fig. 5. PXRD patterns of (a) SGP-0.3-300, (b) SGP-0.3-400 and (c) SGP-0.3-500. Reflections of anatase and rutile are indicated, respectively.

and the interface between crystallites [1–4,6–16]. To study the influences of the heat treatment, the sample SGP-0.3 was chosen to be heated in air at 300, 400 or 500 °C. Fig. 5 shows the PXRD patterns of the resulting SGP-0.3-*T* samples. The reflections of rutile become narrower and more intense with increasing the heating temperature, suggesting that part of the anatase phase was thermally transformed to rutile accompanying with sintering of the original rutile nanocrystals. The crystallite size of rutile phase increased to ~10 nm for SGP-0.3-300 and to ~21 nm for SGP-0.3-500. SEM and TEM images of the heated samples are shown in Fig. 6. The flower-like morphology is preserved in SGP-0.3-300 but the diameter of the needle-shaped nanorods becomes a bit larger (~9 nm), but the rods in SGP-0.3-500 become 40 nm in width and are pure-rutile (suggested by SAED). Consistent with the observed morphological evolution, the surface area is 121 $m^2 g^{-1}$ for SGP-0.3-300 and is dramatically decreased to 53 $m^2 g^{-1}$ for SGP-0.3-500.

The effects of the heat treatment on the UV–visible absorption of the mixed-phase TiO_2 nanostructures were also studied, and the absorption spectra of selected samples are shown in Fig. 7. All the materials absorb strongly in the UV regime, and the absorption thresholds for 3D TiO_2 nanostructures are red-shifted as compared to that for P25. The band gaps estimated from the absorption thresholds [60] are 3.19 eV for P25, 3.11 eV for SGP-0.3 and around 3.04–3.05 eV for all the heated SGP-0.3-*x* samples. The microwave-synthesized sample mSGP-0.3-300 also has a band gap of 3.05 eV, but the value for ST21-seeded sample SGS-0.3-300 is a bit higher (3.07 eV), probably due to a higher content of anatase. Interestingly, SGP-0.3-300 also exhibits weak absorption extended to the visible light regime (>400 nm), a phenomenon probably related to the presence of the localized Anderson states at the anatase/rutile interface [61]. Similar phenomenon has been observed for mixed-phase TiO_2 film fabricated by aerosol deposition [62].

Finally, the photocatalytic activities of the mixed-phase TiO_2 nanostructures were evaluated. Methylene blue (MB) is a frequently used model organic pollutant in semiconductor photocatalysis [13] and was chosen in this study. The power density of the UV irradiation was kept low (1.7 mW cm^{-2}) to prevent possible multiphoton processes or serious UV absorption of the dye molecules. MB solution was oxygen-saturated and the solution pH was adjusted at pH 6.5 to prevent possible photobleaching of the dye by reduction [49,63]. Prior to the UV irradiation, all

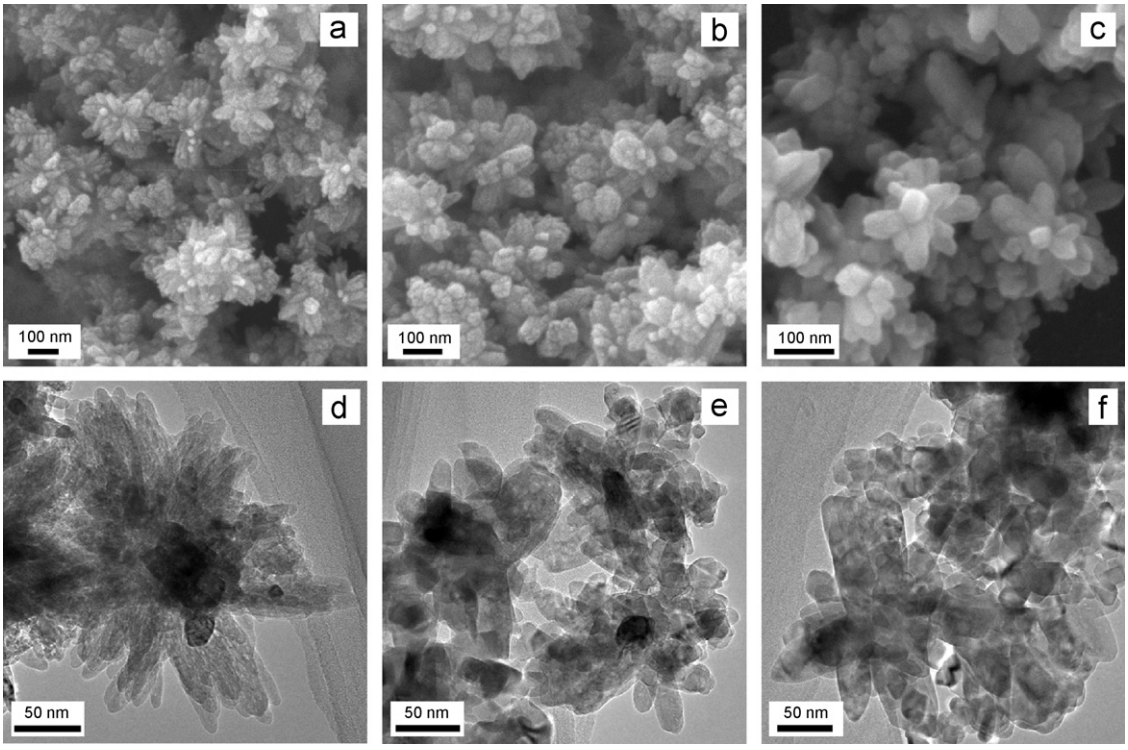

Fig. 6. SEM and TEM images of (a, d) SGP-0.3-300, (b, e) SGP-0.3-400 and (c, f) SGP-0.3-500.

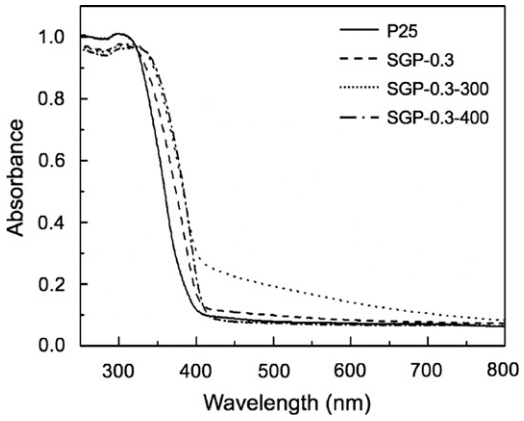

Fig. 7. UV–visible absorption spectra of selected samples.

the TiO_2 samples were stirred in the dark and showed low adsorption of MB, suggesting a weak MB–TiO_2 interaction in the reaction solution. Fig. 8a compares the curves of the change in relative concentration of MB versus irradiation time in the presence of different TiO_2 samples. The amounts of the self-degraded dye [49] (cf. the curve labeled "MB" in Fig. 8) were taken into consideration when evaluating the activity of the photocatalysts. For P25, about 47% of MB was decomposed after UV irradiation for 360 min. After the same duration of UV irradiation, SGP-0.3 only decomposed ~13% of MB but the heated sample (SGP-0.3-*x*) degraded much more (74–88%) dye. Furthermore, the transformed logarithm plots in Fig. 8b show the linear relationship between $\ln(C/C_0)$ and time for all the TiO_2 catalysts, suggesting that the overall kinetics of the photodecomposition reactions was first-order with respect to the concentration of MB. Fig. 9 compares the derived apparent rate constants (k_{app}) for P25, SGP-0.3-series samples and other selected samples. Among all the

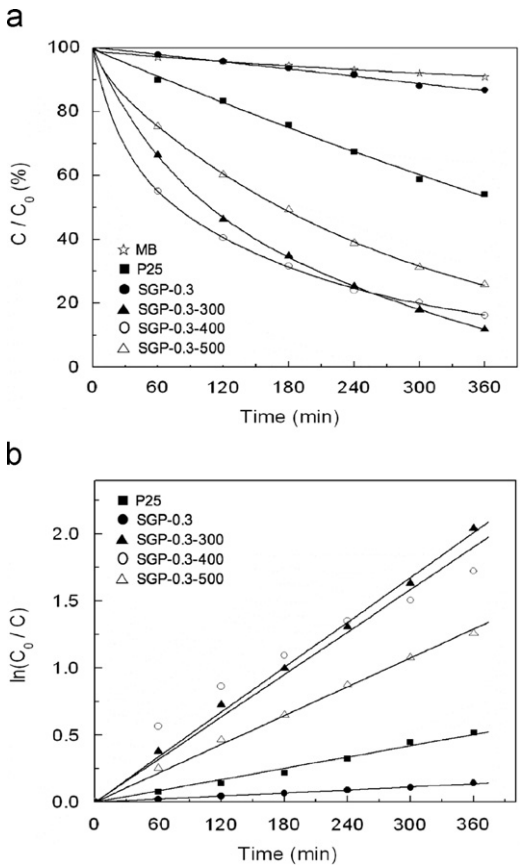

Fig. 8. (a) Change in relative concentration of MB with UV irradiation time in the presence of photocatalysts. The curve of the control experiment without adding any catalyst is labeled "MB". (b) Transformed linear graph of $\ln(C_0/C)$ versus irradiation time.

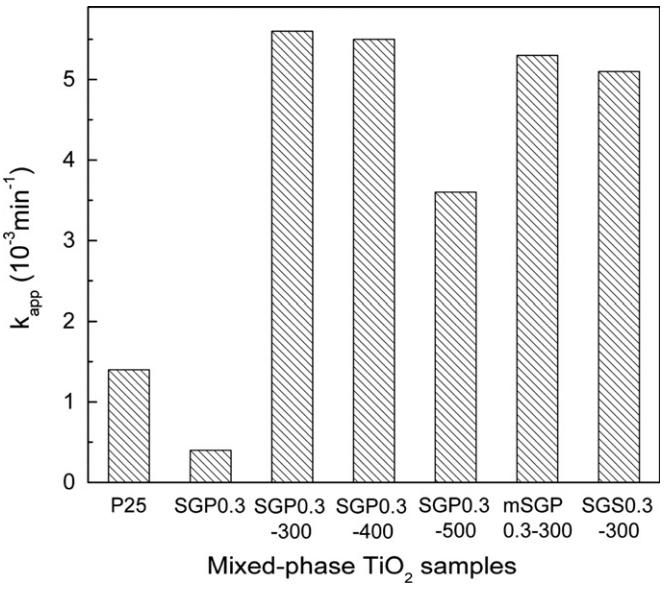

Fig. 9. Comparison of apparent first-order rate constants of MB photodegradation for selected samples.

catalysts, SGP-0.3-300 and SGP-0.3-400 exhibited the highest k_{app} of 5.5–5.6 $\times 10^{-3}$ min^{-1}, which is much larger than that for P25 (1.4×10^{-3} min^{-1}) or SGP-0.3 (0.4×10^{-3} min^{-1}). By using P25 as a standard photocatalyst for comparison, we found that SGP-0.3-300 is even more active than other mixed-phase TiO_2 materials [18,54–57]. Besides, the k_{app} values for microwave-synthesized mSGP-0.3-300 and the ST21-seeded SGS-0.3-300 are also high and comparable to those for SGP-0.3-300 and SGP-0.3-400. The high photocatalytic activities of these samples may be associated to the high surface area and unique anisotropic mixed-phase nanostructures. It was found by Gray and coworkers that although the energy position of the conduction band edge of anatase is higher than that of rutile, the photogenerated electron actually migrate from rutile to lower-energy trapping sites in anatase and at anatase–rutile interface [17,20]. Such a synergistic effect has been reported for P25 and other mixed-phase TiO_2 [19–23]. We speculate that the TiO_2 nanostructures with the anisotropic mixed-phases might have high density of anatase/rutile interface, and pronounced synergistic effect might contribute to the high photoactivities of these materials.

4. Conclusion

We have developed a simple and high-yield nonaqueous seeded growth of flower-like mixed-phase TiO_2 nanostructures. The synthesis does not need any structure-directing or capping agents and can be accelerated by applying a microwave heating. The TiO_2 nanostructures have unique anisotropic mixed-phase structure and high surface area. After suitable heat treatment, the nanostructures may exhibit high photocatalytic activities, as examined by the photodegradation of methylene blue. The results demonstrate the uniqueness of the nonaqueous seeded growth and the potential of the thus prepared TiO_2 nanostructures for practical applications.

Acknowledgment

The authors thank the National Science Council of the Republic of China for financial support under the Contract no. NSC98-2113-M-007-020-MY3.

References

[1] B. O'Regan, M. Grätzel, Nature 353 (1991) 737.
[2] M.K. Nazeeruddin, P. Péchy, T. Renouard, S.M. Zakeeruddin, R. Humphry-Baker, P. Comte, P. Liska, L. Cevey, E. Costa, V. Shklover, L. Spiccia, G.B. Deacon, C.A. Bignozzi, M. Grätzel, J. Am. Chem. Soc. 123 (2001) 1613.
[3] M. Grätzel, Acc. Chem. Res. 42 (2009) 1788.
[4] G. Li, C.P. Richter, R.L. Milot, L. Cai, C.A. Schmuttenmaer, R.H. Crabtree, G.W. Brudvig, V.S. Batista, Dalton Trans. (2009) 10078.
[5] T. Wakanabe, A. Kitamura, E. Kojima, C. Nakayama, K. Hashimoto, A. Fujishima, Photocatalytic Purification and Treatment of Water and Air, Elsevier, Amsterdam, 1993.
[6] M.R. Hoffmann, S.T. Martin, W. Choi, D.W. Bahnemann, Chem. Rev. 95 (1995) 69.
[7] A.L. Linsebigler, G. Lu, J.T. Yates, Chem. Rev. 95 (1995) 735.
[8] G.J.A.A. Soler-Illia, J. Patarin, B. Lebeau, C. Sanchez, Chem. Rev. 102 (2002) 4093.
[9] F. Schüth, Angew. Chem. Int. Ed. 42 (2003) 3604.
[10] M.H. Bartl, S.W. Boettcher, K.L. Frindell, G.D. Stucky, Acc. Chem. Res. 38 (2005) 263.
[11] M.R. Hoffmann, J. Phys. Chem. B 109 (2005) 8673.
[12] T. Thompson, J. Yates Jr., Chem. Rev. 106 (2006) 4428.
[13] O. Carp, C.L. Huisman, A. Reller, Prog. Solid State Chem. 32 (2004) 33.
[14] X. Chen, S.S. Mao, Chem. Rev. 107 (2007) 2891.
[15] C. Aprile, A. Croma, H. Carcia, Phys. Chem. Chem. Phys. 10 (2008) 769.
[16] H. Zhang, G. Chen, D.W. Bahnemann, J. Mater. Chem. 19 (2009) 5089.
[17] D.C. Hurum, A.G. Agrios, S.E. Crist, K.A. Gray, T. Rajh, M.C. Thurnauer, J. Electron Spectrosc. Relat. Phenom. 150 (2006) 155.
[18] G. Li, L. Chen, M.E. Graham, K.A. Gray, J. Mol. Catal. A: Chem. 275 (2007) 30.
[19] T. Ohno, K. Tokieda, S. Higashida, M. Matsumura, Appl. Catal. A: Gen. 244 (2003) 383.
[20] D.C. Hurum, A.G. Agrios, K.A. Gray, T. Rajh, M.C. Thurnauer, J. Phys. Chem. B 107 (2003) 4545.
[21] M. Yan, F. Chen, J. Zhang, M. Anpo, J. Phys. Chem. B 109 (2005) 8673.
[22] G. Li, S. Ciston, Z. Saponjic, L. Chen, N. Dimitrijevic, T. Rajh, K.A. Gray, J. Catal. 253 (2008) 105.
[23] G. Li, C.P. Richter, R.L. Milot, L. Cai, C.A. Schmuttenmaer, R.H. Crabtree, G.W. Brudvig, V.S. Batista, Dalton Trans. (2009) 10078.
[24] P. Yang, D. Zhao, D. Margolese, B.F. Chmelka, G.D. Stucky, Nature 396 (1998) 152.
[25] B. Tian, H. Yang, X. Liu, S. Xie, C. Yu, J. Fan, B. Tu, D. Zhao, Chem. Commun. (2002) 1824.
[26] Y. Yin, P. Alivisatos, Nature 437 (2005) 664.
[27] D.V. Bavykin, J.M. Friedrich, F.C. Walsh, Adv. Mater. 18 (2006) 2807.
[28] Y. Mao, T.J. Park, F. Zhang, H. Zhou, S.S. Wong, Small 3 (2007) 1122.
[29] C.J. Brinker, G.W. Scherer, Sol–Gel Science, Academic Press, San Diego, 1990.
[30] J. Livage, M. Henry, C. Sanchez, Prog. Solid State Chem. 18 (1988) 259.
[31] L.L. Hench, J.K. West, Chem. Rev. 90 (1990) 33.
[32] E. Matijevic, Pure Appl. Chem. 64 (1992) 1703.
[33] E. Matijevic, Langmuir 10 (1994) 8.
[34] A. Vioux, Chem. Mater. 9 (1997) 2292.
[35] J.N. Hay, H.M. Raval, Chem. Mater. 13 (2001) 3396.
[36] M. Inoue, J. Phys. Condens. Matter 16 (2004) S1291.
[37] B.L. Cushing, V.L. Kolesnichenko, C.J. O'Connor, Chem. Rev. 104 (2004) 3893.
[38] M. Niederberger, G. Garnweitner, Chem. Eur. J. 12 (2006) 7282.
[39] M. Niederberger, Acc. Chem. Res. 40 (2007) 793.
[40] M. Niederberger, M.H. Bartl, G.D. Stucky, Chem. Mater. 14 (2002) 4364.
[41] M. Niederberger, M.H. Bartl, G.D. Stucky, J. Am. Chem. Soc. 124 (2002) 13642.
[42] G. Garnweitner, M. Niederberger, J. Mater. Chem. 18 (2008) 1171.
[43] T. Tsumura, N. Kojitani, I. Izumi, N. Iwashita, M. Toyoda, M. Inagaki, J. Mater. Chem. 12 (2002) 1391.
[44] L. Lin, W. Lin, Y.X. Zhu, B.Y. Zhao, Y.C. Xie, Y. He, Y.F. Zhu, J. Mol. Catal. A: Chem. 236 (2005) 46.
[45] B. Tryba, A.W. Morawski, T. Tsumura, M. Toyoda, M. Inagaki, J. Photochem. Photobiol. A: Chem. 167 (2004) 127.
[46] T. Matsunaga, M. Inagaki, Appl. Catal. B: Environ. 64 (2006) 9.
[47] H. Zhang, J.F. Banfield, J. Phys. Chem. B 104 (2000) 3481.
[48] A. Mills, S. LeHunte, J. Photochem. Photobiol. A 108 (1997) 1.
[49] Y.C. Hsu, H.C. Lin, C.W. Lue, Y.T. Liao, C.M. Yang, Appl. Catal. B: Environ. 89 (2009) 309.
[50] C.C. Wang, J.Y. Ying, Chem. Mater. 11 (1999) 3113.
[51] C. Wang, Z.X. Deng, Y.D. Li, Inorg. Chem. 40 (2001) 5210.
[52] W.P. Huang, X.H. Tang, Y.Q. Wang, Y. Koltypin, A. Gedanken, Chem. Commun. (2000) 1415.
[53] M.M. Wu, G. Lin, D.H. Chen, G.G. Wang, D. He, S.H. Feng, R.R. Xu, Chem. Mater. 14 (2002) 1974.
[54] J.M. Wu, B. Qi, J. Phys. Chem. C 111 (2007) 666.
[55] Y. Mao, M. Kanungo, T.H. Benny, S.S. Wong, J. Phys. Chem. B 110 (2006) 702.
[56] G. Wu, J. Wang, D.F. Thomas, A. Chen, Langmuir 24 (2008) 3503.
[57] S. Bakardjieva, V. Stengl, L. Szatmary, J. Subrt, J. Lukac, N. Murafa, D. Niznansky, K. Cizek, J. Jirkovsky, N. Petrova, J. Mater. Chem. 16 (2006) 1709.

[58] M. Niederberger, G. Garnweitner, F. Krumeich, R. Nesper, H. Cölfen, M. Antonietti, Chem. Mater. 16 (2004) 1202.
[59] J. Polleux, N. Pinna, M. Antonietti, C. Hess, U. Wild, R. Schlög, M. Niederberger, Chem. Eur. J. 11 (2005) 3541.
[60] H. Tang, K. Prasad, R. Sanjinès, P.E. Schmid, F. Lévy, J. Appl. Phys. 75 (1994) 2042.
[61] R.I. Bickley, T. Gonzalezcarreno, J.S. Lees, L. Palmisano, R.J.D. Tilley, J. Solid State Chem. 92 (1991) 178.
[62] J. Ryu, D.S. Park, B.D. Hahn, J.J. Choi, W.H. Yoon, K.Y. Kim, H.S. Yun, Appl. Catal. B: Environ. 83 (2008) 1.
[63] A. Mills, J. Wang, J. Photochem. Photobiol. A: Chem. 127 (1999) 123.